In situ Preparation of Co_4S_3-based Electrocatalyst by Taking Advantage of Controllable Components of Metal-Organic Frameworks

Tang-ming Li,[a, ‡] Bing-qian Hu,[a, ‡] Jing-hua Han,[a] Wangting Lu,[a] Fan Yu,[a,*] Bao Li[b,*]

[a] Key Laboratory of Optoelectronic Chemical Materials and Devices of Ministry of Education, School of Chemical and Environmental Engineering, Jianghan University, Wuhan, Hubei 430056, People's Republic of China. Email : yufan0714@163.com;

[b] School of Chemistry and Chemical Engineering, Hubei Key Laboratory of Bioinorganic Chemistry&Materia Medica, Huazhong University of Science and Technology, Wuhan, Hubei 430074, People's Republic of China.Email: libao@hust.edu.cn

1. Experimental section

Materials and General Methods

The organic ligands were used as received from commercial sources without further purification. Powder X-ray diffraction (PXRD) was carried out on a Bruker D8-Focus Bragg-Brentano X-ray Powder Diffractometer equipped with a Cu sealed tube (λ = 1.54178 Å) at 40 kV and 40 mA. Thermogravimetry analysis (TGA) was conducted on a TGA-50 thermogravimetric analyzer. The morphology was observed with a Sigma HD Thermal field emission scanning electron microscope (SEM). The elemental composition of the samples were characterized by energy-dispersive X-ray spectroscopy (EDS, Oxford instruments X-Max). The X-ray photoelectron spectroscopy (XPS) spectras were collected by Thermo ESCALAB 250XI spectrometer.

Synthesis of Co-MOF-1: $CoSO_4 \cdot 7H_2O$ (0.1 mmol) and KSCN (0.2 mmol) were stirred in 5 ml methanol for 5 minutes, then the solution was filtered and 1 ml water was added to the filtrate. The resulting solution was placed in a test tube, above which layered 5 ml methanol, and then 5 ml methanol containing 0.025 mmol L2 was layered on the top. After one week, glittering pink crystal were obtained (40% based on L2). The reaction image is shown in Figure S1.

Synthesis of Co-MOF-2: $CoSO_4 \cdot 7H_2O$ (0.1 mmol) and KSCN (0.2 mmol) were stirred in 5 ml methanol for 5 minutes, then the solution was filtered and 1 ml DMF was added to the filtrate. The resulting solution was placed in a test tube, above which layered 5 ml methanol, and then 5 ml methanol containing 0.025 mmol L2 was layered on the top. After one week, glittering pink crystal were obtained (35% based on L2). The reaction image is shown in Figure S1.

Synthesis of Co-MOF-1 based derivatives: Weigh 150 mg of grounded Co-MOF-1 precursor and lay it in a clean quartz boat (evenly spread to prevent agglomeration), put it in the center of the quartz tube, and screw down the screws fixing the quartz tube. Open the nitrogen valve, inject nitrogen as protective gas, and adjust the flowmeter to the maximum for 30 min to ensure that the residual oxygen in the quartz tube is discharged. Then raise the temperature to 400 ℃ at the rate of 5 ℃ min^{-1}, keep

the sample in the quartz boat heated for 2 hours, naturally drop to room temperature, close the nitrogen valve and take out the sample. The obtained Co-MOF-1 derivative was named Co-MOF-1-400. Other conditions remained unchanged, and the calcination temperatures were changed to 500 ℃, 600 ℃ and 700 ℃, which were named Co-MOF-1-500, Co-MOF-1-600 and Co-MOF-1-700 respectively.

Synthesis of Co-MOF-2 based derivatives: The synthesis route is similar to Co-MOF-1 series excepted for the template is Co-MOF-2. Weigh 150 mg of grounded Co-MOF-2 precursor and lay it in a clean quartz boat (evenly spread to prevent agglomeration), put it in the center of the quartz tube, and screw down the screws fixing the quartz tube. Open the nitrogen valve, inject nitrogen as protective gas, and adjust the flowmeter to the maximum for 30 min to ensure that the residual oxygen in the quartz tube is discharged. Then raise the temperature to 400 ℃ at the rate of 5 ℃ min^{-1}, keep the sample in the quartz boat heated for 2 hours, naturally drop to room temperature, close the nitrogen valve and take out the sample. The obtained Co-MOF-2 derivative was named Co-MOF-2-400. Other conditions remained unchanged, and the calcination temperatures were changed to 500 ℃, 600 ℃ and 700 ℃, which were named Co-MOF-2-500, Co-MOF-2-600 and Co-MOF-2-700 respectively.

Electrochemical measurements and products analysis.

Electrochemical measurements were carried out with a computer-controlled CHI 760E electrochemistry workstation at room temperature. A three-electrode system consisting of a working electrode (5.0 mm in diameter), a saturated calomel electrode (SCE), and a graphite rod counter electrode was used. The working electrode was a glassy carbon electrode coated with a thin layer of catalyst, which was prepared by ultrasonically mixing 5.0 mg of the as-prepared catalyst with 30 μL of NaOH on solution and 500 μL of ethanol solvent for 30 min in order to form a catalyst ink. Then, 20.0 μL of the prepared catalyst ink was loaded onto the surface of a glassy carbon electrode of 5.0 mm diameter using a micropipette. Finally, the ink was allowed to dry overnight under ambient conditions to form a thin catalyst film. To improve the conductivity, the obtained samples were mixed with 30 wt% of carbon powders (Cabot Vulcan XC72) while fixing the weight of the total catalyst mixture. Catalyst

loading is approximately 0.672 mg cm^{-2} on the glassy carbon electrode. For comparison, the electrocatalytic performance of the benchmark IrO_2 was also investigated under the same conditions. Voltammetry studies were performed in 1.0 M aqueous KOH electrolyte. Linear sweep voltammetry was performed at a scan rate of 5 mV s^{-1}. All the polarization curves of the oxygen evolution reaction were *iR*-corrected. Unless otherwise stated, all potentials were converted to the reversible hydrogen electrode (RHE) potential in all measurements. In 1.0 M KOH solution, the potential of the SCE was calibrated as +1.067 V with respect to the RHE. Electrochemical impedance spectroscopy (EIS) in the range of 100000 ~0.1Hz was analyzed. When the current density was 10mA cm^{-2}, the stability of the catalyst was tested by chronopotentiometry method.

Table S1. the typical IR peaks in different samples

Unit：cm^{-1}	＝C－H	C＝C	C－S	$-CH_2$	－NH
Co-MOF-1	3057.1	1575.4	1234.6	1428.0	3069.2
Co-MOF-1-400	-	1630.7	1066.1	-	3209.5
Co-MOF-1-500	-	1543.3	1065.7	-	3194.5
Co-MOF-1-600	-	1631.4	1070.4	-	3208.4
Co-MOF-1-700	-	1543.4	1066.3	-	3152.0

Unit：cm^{-1}	＝C－H	C＝C	C－S	$-CH_2$	－NH
Co-MOF-2	-	1574.6	1234.6	1427.5	-
Co-MOF-2-400	-	1547.0	1067.6	-	3196.3
Co-MOF-2-500	-	1632.0	1067.0	-	3204.5
Co-MOF-2-600	-	1636.2	1070.3	-	3195.1
Co-MOF-2-700	-	1630.0	1066.1	-	3198.2

Table S2. The related electrocatalytic performances of Co-MOF-1 series

	Current density mA·cm-2	Co-MOF-1 mV	Co-MOF-1-400 mV	Co-MOF-1-500 mV	Co-MOF-1-600 mV	Co-MOF-1-700 mV
OER	10	357	262	319	325	321
	100	432	292	400	408	420
HER	10	311	292	260	261	305
	100	460	396	390	394	455

Table S3. The related electrocatalytic performances of Co-MOF-2 series

	Current density mA· m^{-2}	Co-MOF-2 mV	Co-MOF-2-400 mV	Co-MOF-2-500 mV	Co-MOF-2-600 mV	Co-MOF-2-700 mV
OER	10	354	339	333	324	323
	100	474	435	447	-	-
HER	10	290	225	298	280	266
	100	459	378	438	-	395

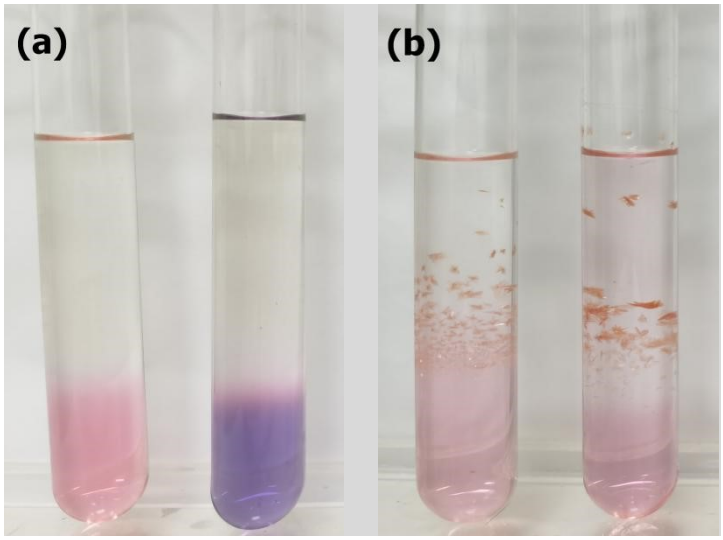

Figure S1. The reaction images of preparing Co-MOF-1(left) and Co-MOF-2 (right) at the beginning and after one weeks

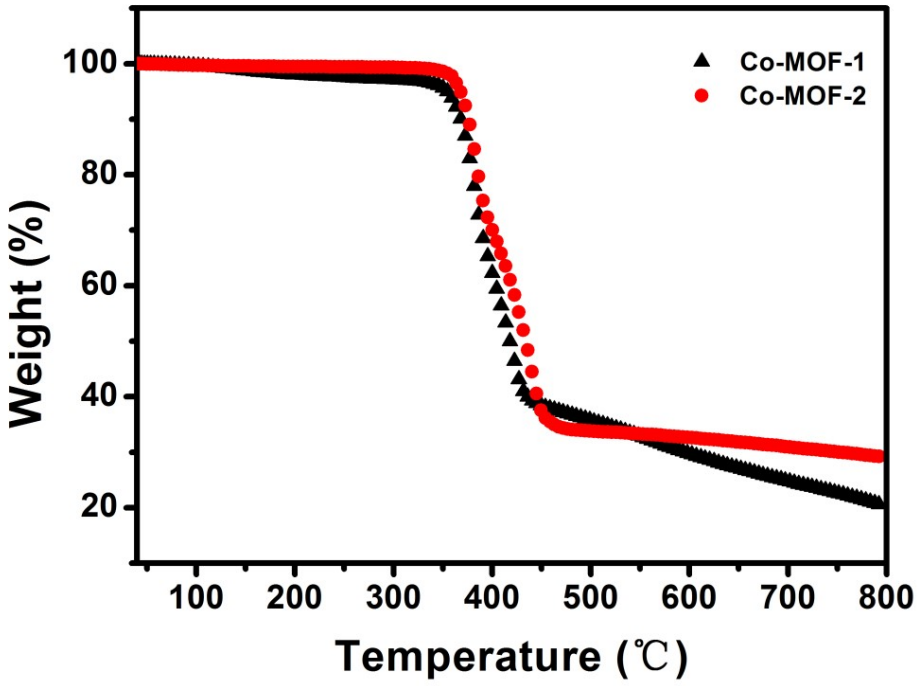

Figure S2. TGA curves of Co-MOF-1 and Co-MOF-2

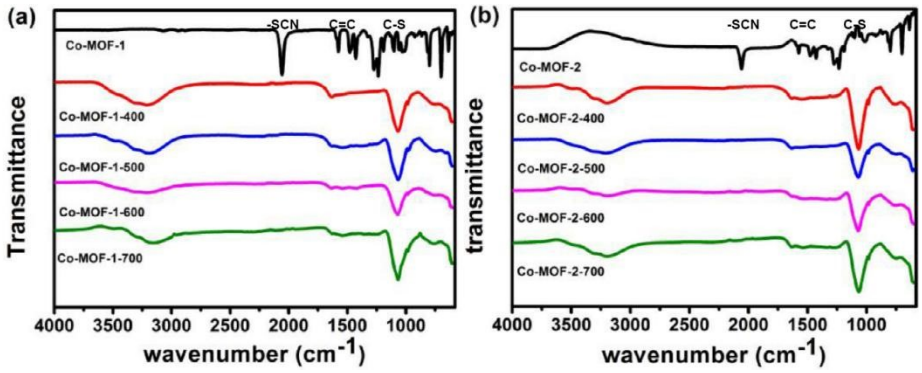

Figure S3. IR spectra of series of derivatives

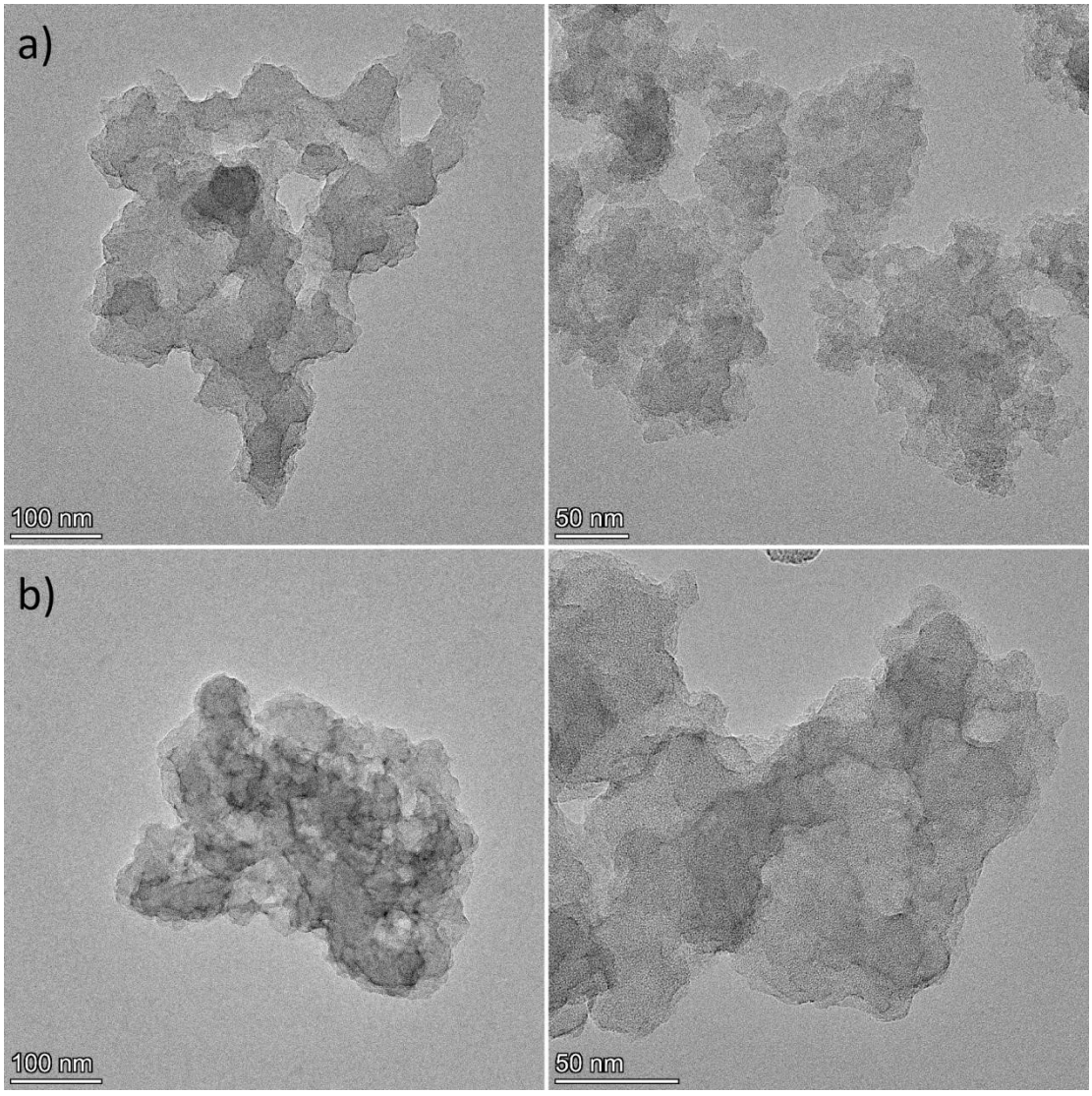

Figure S4. TEM of Co-MOF-1-400(a) and Co-MOF-2-400(b) with 100 nm and 50 nm scale.

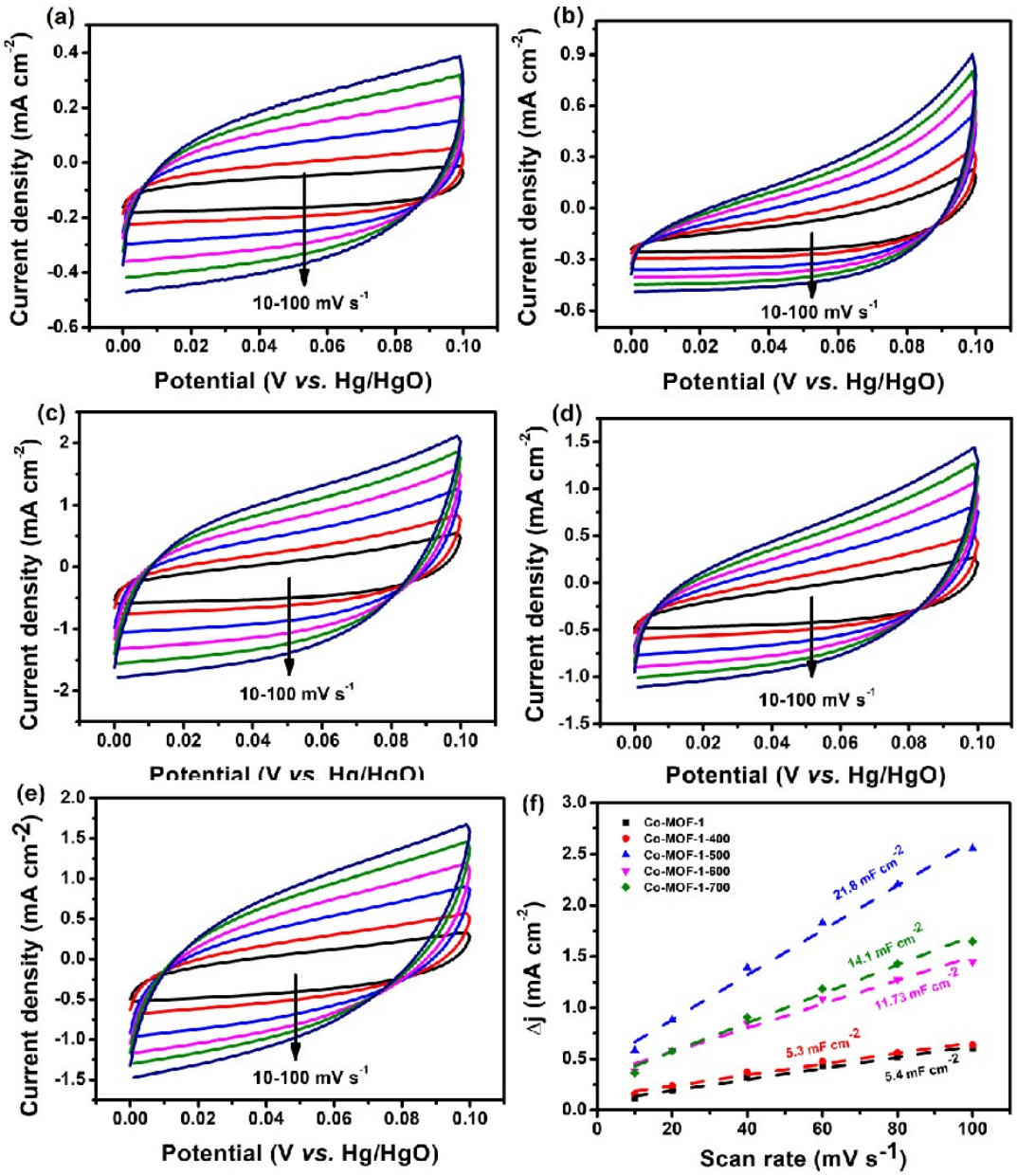

Figure S5. Cyclic voltammetry of curves (a-e) and electrochemical double-layer capacitance (f) of Co-MOF-1, Co-MOF-1-400, Co-MOF-1-500, Co-MOF-1-600, and Co-MOF-1-700 at different scan rates (10, 20, 40, 80 and100 mV s^{-1}).

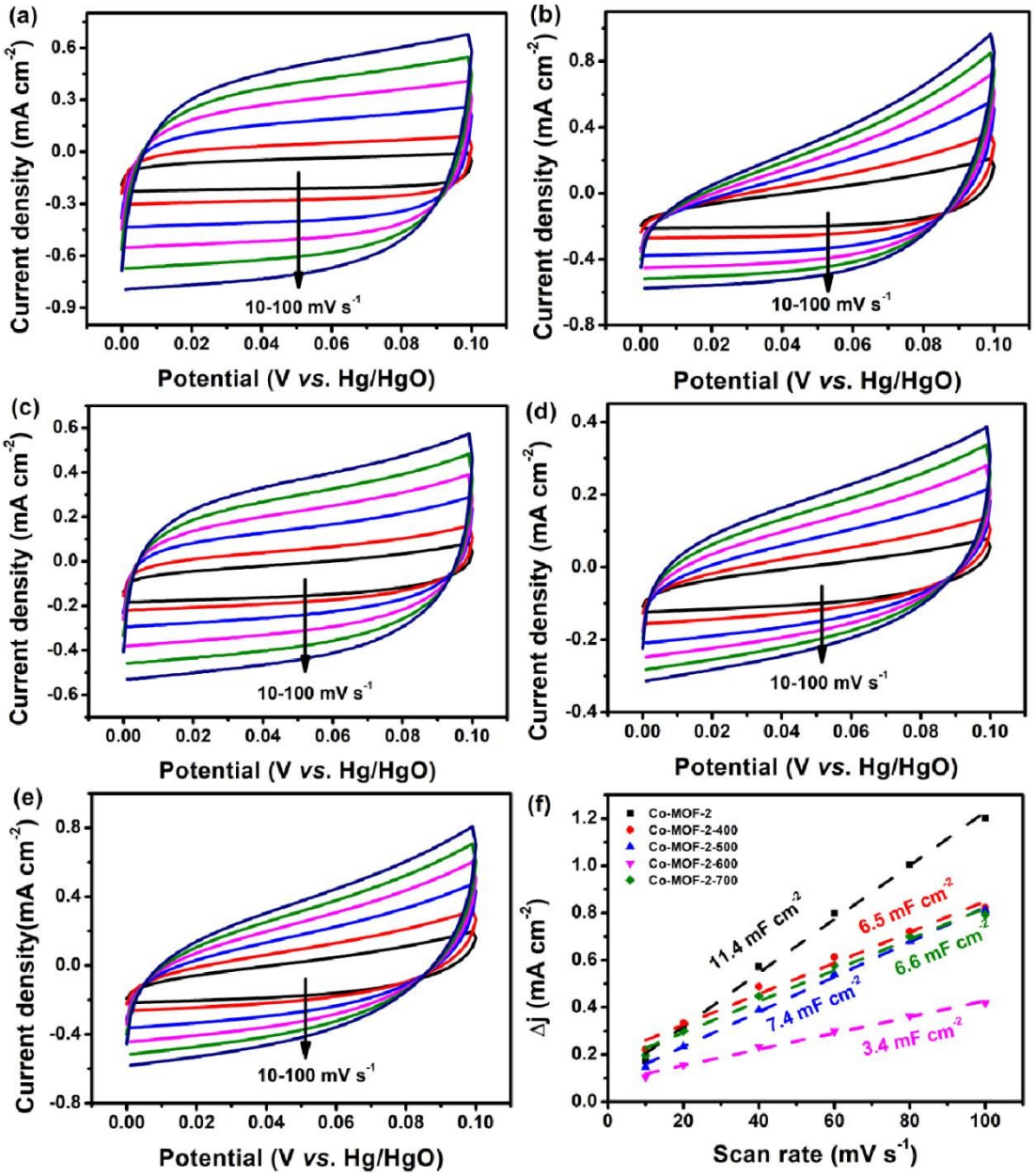

Figure S6. Cyclic voltammetry of curves (a-e) and electrochemical double-layer capacitance (f) of Co-MOF-2, Co-MOF-2-400, Co-MOF-2-500, Co-MOF-2-600, and Co-MOF-2-700 at different scan rates (10, 20, 40, 80 and100 mV s^{-1})

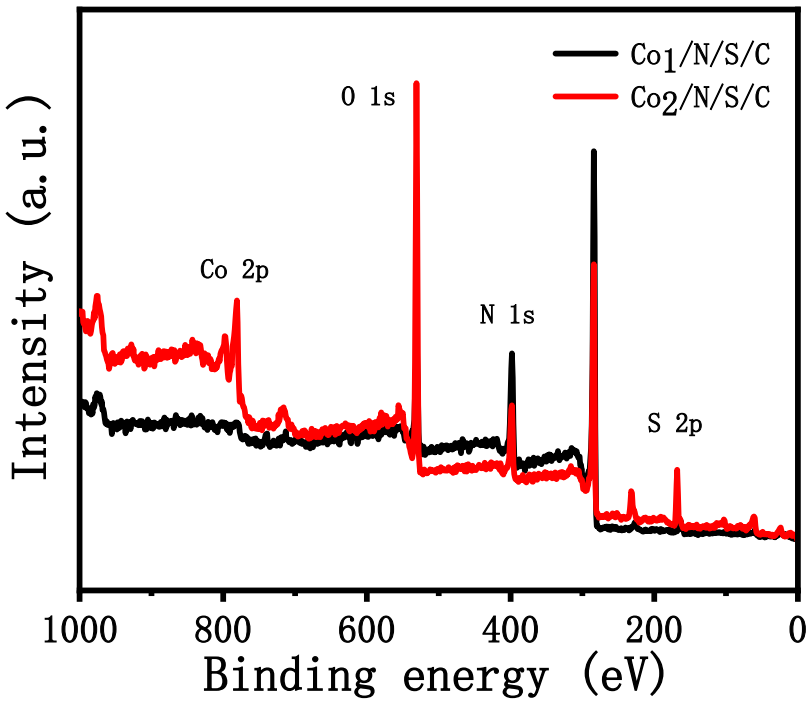

Figure S7. The overall XPS spectra of Co-MOF-1-400 and Co-MOF-2-400.

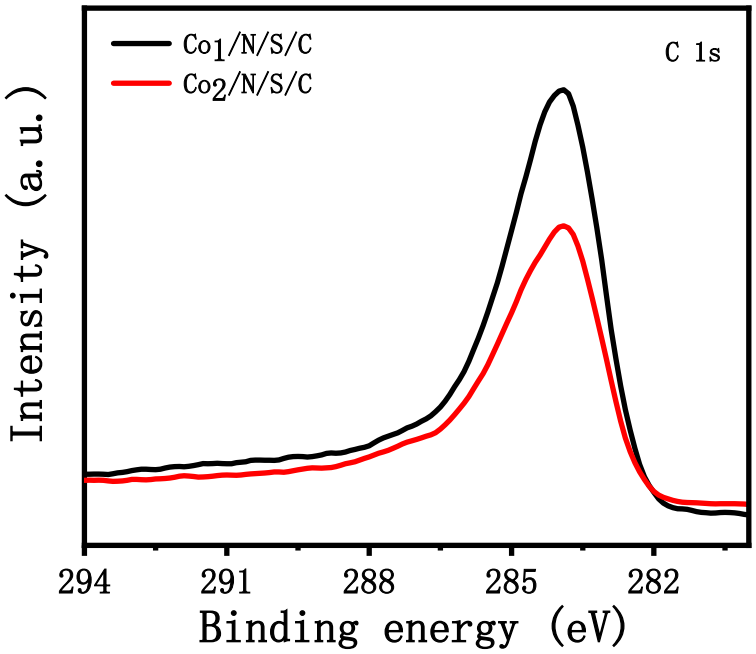

Figure S8. The C spectra of Co-MOF-1-400 and Co-MOF-2-400.

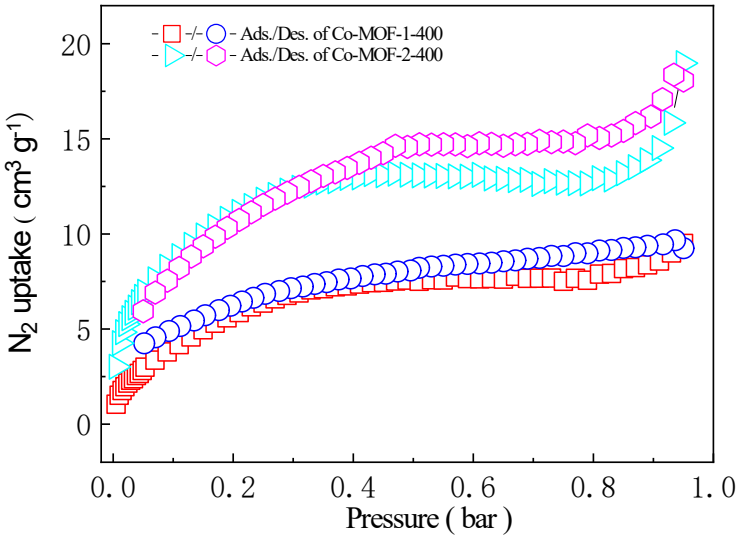

Figure S9. N_2 sorption isotherms for Co-MOF-1-400 and Co-MOF-2-400.

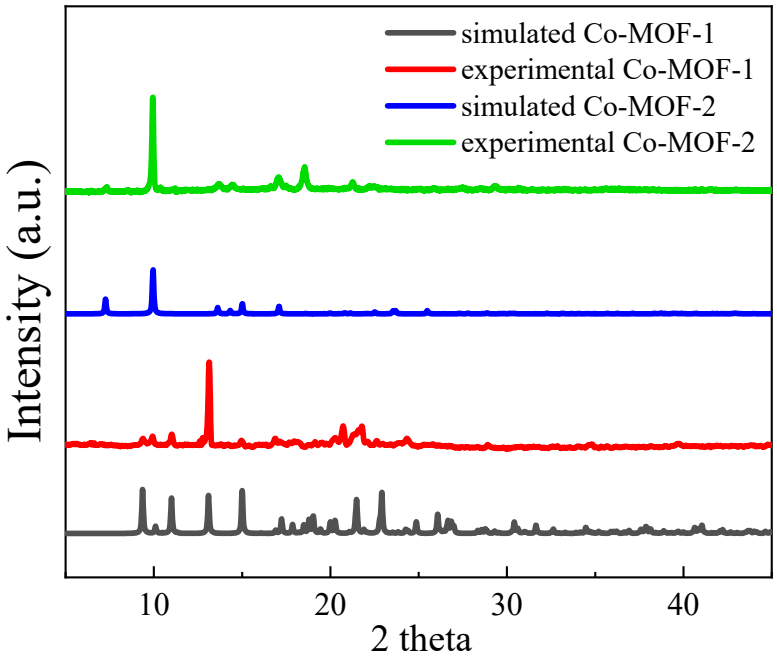

Figure S10. XRD patterns for pristine Co-MOF-1 and Co-MOF-2.

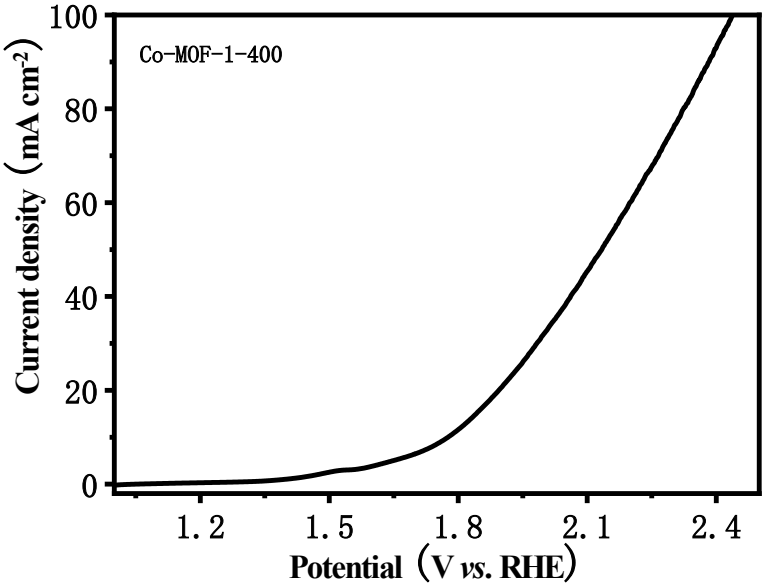

(a)

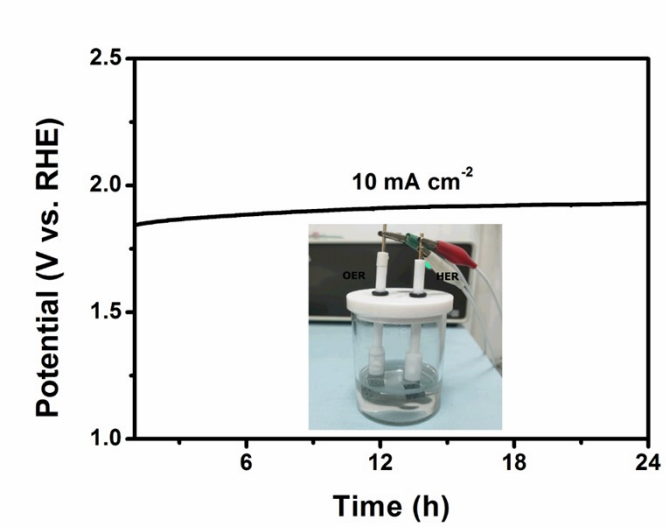

(b)

Figure S11. The reaction of over-all water splitting with the utilization of Co-MOF-1-400 as HER and OER catalyst (a) and stability experiment (b).

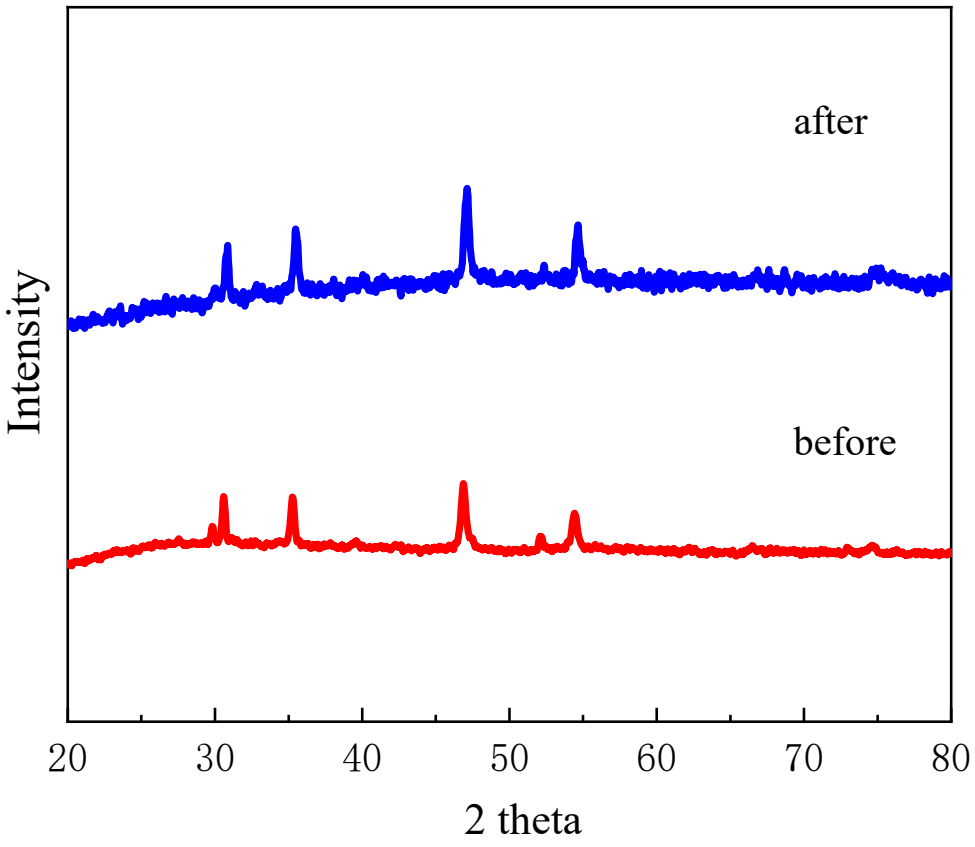

Figure S12. XRD patterns for Co-MOF-1-400 before and after the catalytic reaction.

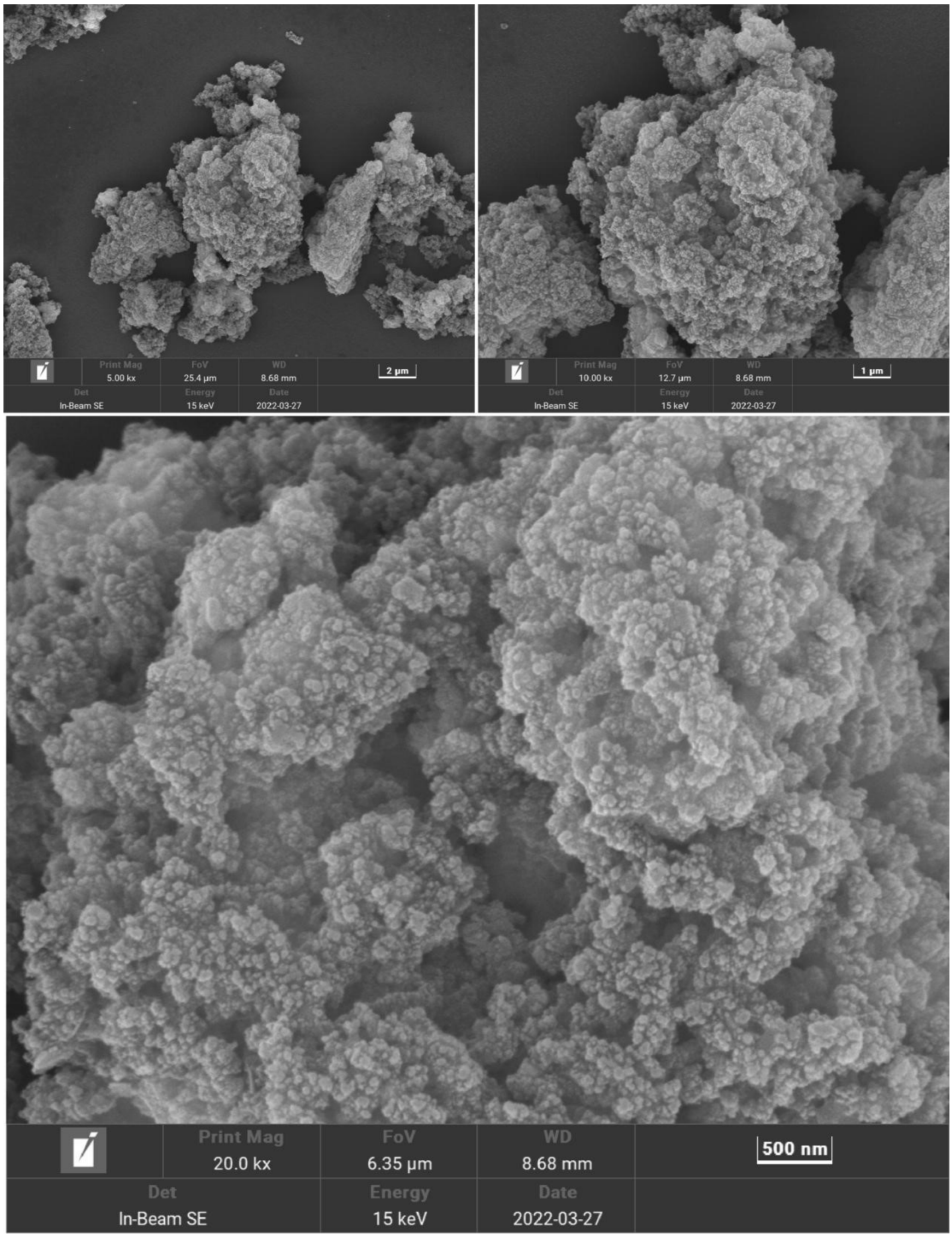

Figure S13. SEM of Co-MOF-1-400 after catalytic experiments.

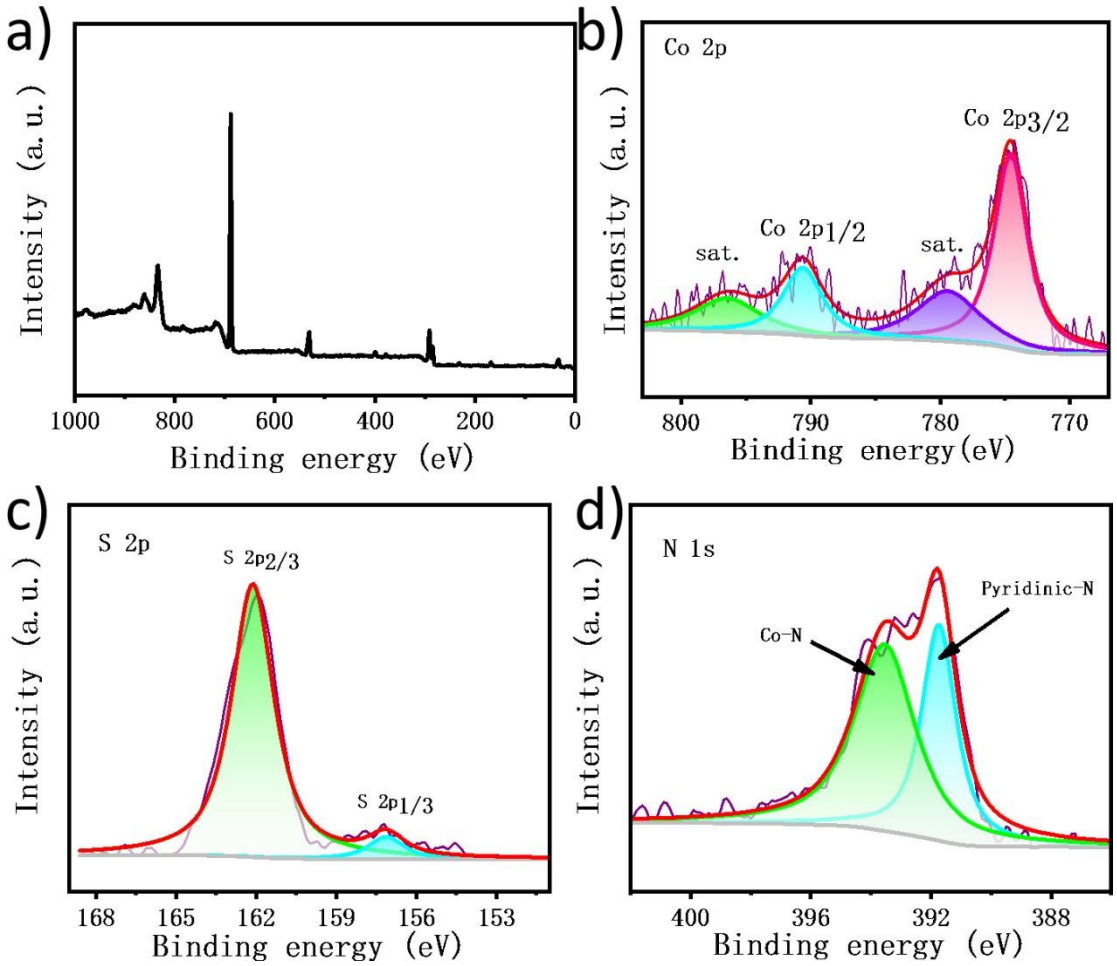

Figure S14. XPS of Co-MOF-1-400 after catalytic experiments.

Table S4. The list of some reported Co/S derivatives as OER catalysts

Sample	OER (η_{10}, mV vs. RHE)	Reference
Co/N/S/C-400	***262***	***This work***
Co_9S_8/NSCP	370	*Chem. Eng. J.* **2022**，431，133385 [S1]
Co_9S_8/GN	450	*ACS Appl. Mater. Interfaces* **2020,** 12, 38202 [S2]
Co/Co_9S_8/NSCS	550	*New J. Chem.* **2020,** 44, 9522-9529 [S3]
WN/C@Co_9S_8 @WS_2	560	*Electrochim. Acta* **2020,** 351, 136249 [S4]
Ni_3Fe − Co_9S_8 /rGO	390	*ACS Appl. Mater. Interfaces* **2019,** 11, 4028 [S5]

Co_9S_8/C NSs	434	*Nanoscale* **2019,** 11, 901 [S6]
Co_9S_8/NSG	380	*Nano-Micro Lett.* **2019,** 11, 4 [S7]
NiS_2/CoS_2 - O NWs	240	*Adv. Mater.* **2017,** 29, 1704681 [S8]
$NiCoMnS_4$/N-rGO	410	*Energy Storage Mater.* **2019,** 20, 216 [S9]
Zn - Co - S NN/CFP	330	*ACS Appl. Mater. Interfaces* **2017,** 9, 12574 [S10]
NiO - Al - Co nanosheets	300	*Electrochim. Acta* **2018,** 290, 21[S11]
CoSA+ Co_9S_8/HCNT	330	*Small* **2020,** 16, 1906735[S12]
Co_9S_8@MoS_2-0.5	340	*Inorg. Chem. Front* **2020**, 7, 191 [S13]
Co_9S_8/CeO_2/Co-NC	370	*Nanoscale* **2021,** 13, 3227-3236.[S14]
CoS_x/NCS	330	*Mater. Res. Bull.* **2020,** 125, 110770 [S15]
Co_9S_8@CNT	305	*J. Power Sources* **2020**, 449, 227561[S16]
Co_8FeS_8/CoS@CNT-500	278	*J. Power Sources* **2020**, 449, 227561[S16]
Co_8FeS_8/CoS	292	*J. Power Sources* **2020**, 449, 227561[S16]
Co_9S_8@NS-CNT	302	*Small* **2018**, 14, 1704035[S17]
Co_9S_8/GO	409	*Energy Environ. Sci.***2016**, 9, 1320-1326[S18]
Co_9S_8@Mo2C	293	*ACS Appl. Mater. Interfaces* **2018**, 10, 22291 - 22302[S19]
Co_9S8@TDC	330	*J. Mater. Chem. A* **2019**, 7, 7389-7395[S20]

Reference

[S1] Gao, X.; Xu, Z.; Li, G. MOF-driven ultrafine Co_9S_8 nanocrystals embedded

in N, S-Codoped Multilayer-Assembled carbon nanoplates for efficient bifunctional oxygen electrocatalysis[J]. *Chem. Eng. J.* **2022**, 431, 133385.

[S2] Sun, X.; Gong, Q.; Liang, Y.; Wu, M.; Xu, N.; Gong, P.; Sun, S.; Qiao, J. Exploiting a High-Performance "Double-Carbon" Structure Co_9S_8/GN Bifunctional Catalysts for Rechargeable Zn–Air Batteries. *ACS Appl. Mater. Interfaces* **2020**, 12 (34), 38202-38210.

[S3] Zhang, H.; Niu, F.; Li, S.; Yin, Y.; Dong, H.; Yue, H.; Cao, Z.; Yang, S. Thin Metal Organic Layers Derived Co/Co_9S_8/N, S co-doped Carbon Nanosheets Oxygen Electrocatalysis synthesized by Space Confinement of Montmorillonite. *New J. Chem.* **2020**, 44, 9522-9529.

[S4] Liu, X.; Li, X.; An, M.; Gao, Y.; Cao, Z.; Liu, J. W–N/C@Co_9S_8@WS_2-hollow carbon nanocage as multifunctional electrocatalysts for DSSCS,ORR and OER. *Electrochim. Acta* **2020**, 351, 136249.

[S5] Hu, X.; Huang, T.; Tang, Y.; Fu, G.; Lee, J.-M. Three-Dimensional Graphene-Supported Ni_3Fe/Co_9S_8 Composites: Rational Design and Active for Oxygen Reversible Electrocatalysis. *ACS Appl. Mater. Interfaces* **2019**, 11 (4), 4028-4036.

[S6] Li, L.; Song, L.; Guo, H.; Xia, W.; Jiang, C.; Gao, B.; Wu, C.; Wang, T.; He, J. N-Doped porous carbon nanosheets decorated with graphitized carbon layer encapsulated Co_9S_8 nanoparticles: an efficient bifunctional electrocatalyst for the OER and ORR. *Nanoscale* **2019**, 11 (3), 901-907.

[S7] Shao, Q.; Liu, J.; Wu, Q.; Li, Q.; Wang, H.-g.; Li, Y.; Duan, Q. In Situ Coupling Strategy for Anchoring Monodisperse Co_9S_8 Nanoparticles on S and N Dual-Doped Graphene as a Bifunctional Electrocatalyst for Rechargeable Zn–Air Battery. *Nano-Micro Lett.* **2019**, 11 (1), 4.

[S8] Yin, J.; Li, Y.; Lv, F.; Lu, M.; Sun, K.; Wang, W.; Wang, L.; Cheng, F.; Li, Y.; Xi, P. Oxygen vacancies dominated NiS_2/CoS_2 interface porous nanowires for portable Zn–air batteries driven water splitting devices. *Adv. Mater.* **2017**, 29 (47), 1704681.

[S9] Pendashteh, A.; Sanchez, J. S.; Palma, J.; Anderson, M.; Marcilla, R. Anchored $NiCoMnS_4$ nanoparticles on N-doped rGO: High-performance bifunctional

electrocatalysts for rechargeable Zn-Air batteries. *Energy Storage Mater.* **2019**, 20, 216-224.

［S10］ Wu, X.; Han, X.; Ma, X.; Zhang, W.; Deng, Y.; Zhong, C.; Hu, W. Morphology-controllable synthesis of Zn–Co-mixed sulfide nanostructures on carbon fiber paper toward efficient rechargeable zinc–air batteries and water electrolysis. *ACS Appl. Mater. Interfaces* **2017**, 9 (14), 12574-12583.

［S11］ Tan, P.; Chen, B.; Xu, H.; Cai, W.; He, W.; Ni, M. Growth of Al and Co co-doped NiO nanosheets on carbon cloth as the air electrode for Zn-air batteries with high cycling stability. *Electrochim. Acta* **2018**, 290, 21-29.

［S12］ Li, Y.; Cao, R.; Li, L.; Tang, X.; Chu, T.; Huang, B.; Yuan, K.; Chen, Y. Simultaneously Integrating Single Atomic Cobalt Sites and Co_9S_8 Nanoparticles into Hollow Carbon Nanotubes as Trifunctional Electrocatalysts for Zn–Air Batteries to Drive Water Splitting. *Small* **2020**, 16 (10), 1906735.

［S13］ Li, J.; Li, G.; Wang, J.; Xue, C.; Li, X.; Wang, S.; Han, B.; Yang, M.; Li, L. A novel core–double shell heterostructure derived from a metal–organic framework for efficient HER, OER and ORR electrocatalysis. *Inorg. Chem. Front* **2020**, 7 (1), 191-197.

［S14］ Sun, Y.; Guan, Y.; Wu, X.; Li, W.; Li, Y.; Sun, L.; Mi, H.; Zhang, Q.; He, C.; Ren, X. ZIF-derived" senbei"-like Co_9S_8/CeO_2/Co heterostructural nitrogen-doped carbon nanosheets as bifunctional oxygen electrocatalyst for Zn-air batteries. *Nanoscale* **2021**, 13, 3227-3236.....

［S15］ Ju, Q.; Ma, R.; Pei, Y.; Guo, B.; Liu, Q.; Zhang, T.; Yang, M.; Wang, J. Nitrogen-doped carbon spheres decorated with CoS_x nanoparticles as multifunctional electrocatalysts for rechargeable zn-air battery and overall water splitting. Mater. Res. Bull. **2020**, 125, 110770.

［S16］ Wang, B.; Chen, Y.; Wang, X.; Zhang, X.; Hu, Y.; Yu, B.; Yang, D.; Z hang, W. A microwave-assisted bubble bursting strategy to grow Co_8FeS_8/CoS heterostructure on rearranged carbon nanotubes as efficient electrocatalyst for oxygen evolution reaction[J]. J. Power Sources **2020**, 449, 227561.

［S17］ Wu, L.; Wang, Q.; Li, J.; Yong, Y.; Liu, Y.; Song, S.; Zhang, H. Co_9S_8 Nanoparticles-Embedded N/S-Codoped Carbon Nanofibers Derived from Metal–Orga

nic Framework-Wrapped CdS Nanowires for Efficient Oxygen Evolution Reaction[J]. Small **2018**, 14(20): 1704035.

［S18］ Dou, S.; Tao, L.; Huo, J.; Wang, S.; Dai, L. Etched and doped Co_9S_8/graphene hybrid for oxygen electrocatalysis[J]. *Energy Environ. Sci.* **2016**, 9(4): 1320-1326.

［S19］ Luo, X.; Zhou, Q.; Du, S.; Li, J.; Zhong, J.; Deng, X.; Liu, Y. Porous Co_9S_8/nitrogen, sulfur-doped carbon@ Mo_2C dual catalyst for efficient water splitting[J]. *ACS Appl. Mater. Interfaces* **2018**, 10(26): 22291-22302.

［S20］ Zang, S.; Zhao, J.; Wang, R., Wang, S.; Lv, Y.; Xu, H. Metal–organic framework-derived Co_9S_8 embedded in N, O and S-tridoped carbon nanomaterials as an efficient oxygen bifunctional electrocatalyst[J]. *J. Mater. Chem. A* **2019**, 7(13): 7389-7395.